ALMA Memo 387
ALMA+ACA Simulation Results

J. Pety, F. Gueth, S. Guilloteau
IRAM, Institut de Radio Astronomie Millimétrique
300 rue de la Piscine, F-38406 Saint Martin d'Hères

August 13, 2001

Abstract

This memo describes the simulation results that were presented at the ALMA Configuration Preliminary Design Review, held at IRAM, Grenoble, February 26-27th 2001. A description of the simulation tool can be found in the ALMA memo 386.

The aim of these simulations was to properly assess the impact of the proposed ALMA Compact Array (ACA) on the imaging capabilities of the combined array. For that purpose, it is necessary to perform realistic simulations, including noise and pointing errors. The simulations presented in this memo show that adding the ACA observations does improve the image fidelity, as compared to the ALMA+Single-dish case.

A possible operation scheme of the ALMA+ACA+Single-dish observations is proposed.

1 Introduction

One possibility opened by the prospect of Japan joining the ALMA project is to build an array of smaller antennas (the ALMA Compact Array – ACA), which would hopefully provide enhanced wide-field imaging capabilities by measuring the short spacings, poorly or not sampled by ALMA.

The ALMA field of view is actually quite small, $\sim 27''$ at 230 GHz, and only $\sim 9''$ at 690 GHz. About 25% of the astronomical projects will require larger areas to be mapped (e.g. ISM, molecular outflows, external galaxies, planets), and mosaicing will therefore be an important observational mode. These scientific topics not only require to observe wide fields of view, but also to recover all spatial frequencies, beyond the primary beam scale. The image fidelity is actually completely driven by the inclusion of these large scales. Hence, the ALMA data need to be complemented by short spacings measured by single-dish antennas, and possibly by ACA. The open questions are:

- is ACA useful at all to improve the image quality, as compared to the ALMA + single-dish case?

- if yes, what should be the antenna diameter (6, 7, or 8 m)?
- the number of antennas (within the possibilities left by cost considerations)?
- the configuration?
- the operation modes?

To properly assess the impact of ACA on the imaging capabilities of the combined array, it is necessary to perform realistic simulations, including noise and pointing errors. This document summarizes the results of the simulations that have been performed at IRAM until March 2001. The methods and algorithms used to perform the simulations are described in a separate ALMA memo. The deconvolution is done using a CLEAN-based method.

2 Fidelity estimators

Estimating the quality of the simulated images as compared to the original model is not an easy task: the actual criteria to estimate the observation quality should depend on the science that is to be done... For practical reasons, we used several estimators of the image fidelity, which give a good indication of the overall quality of the observing process.

Fidelity image

The fidelity is defined as the ratio of the input model to the difference (model−simulated image). The higher the fidelity, the better the simulated image. In each particular image and in each particular simulation some pixels happen to have exactly the same intensity in the model and simulated image. Those high fidelity pixels have to be flagged out because they do not reflect the accuracy of the observation, which can only be assessed from a statistical point of view. To insure that the fidelity image is a fair and robust statistical estimator of the imaging quality, we thus impose a threshold to the lowest value of the difference image:

$$\text{fidelity} = \frac{\text{input model}}{\max(\text{difference}, 0.7 \times \text{rms(difference)})}$$

Histogram of cumulated fidelity

To help quantify the visual impression given by the fidelity image, we computed the histogram of cumulated fidelity. It gives the number of pixels in the fidelity image whose values are larger than a given fidelity. Hence, a rectangular shape indicates a fidelity which is homogeneous over the whole image.

Fidelity medians

To further quantify simulation results, we computed fidelity medians. Those quantities have the two following advantages: *(i)* they do not give too much weight to points whose fidelity is coincidentally very high; *(ii)* the inverse of the median is the median of the inverse, which means that this number is also the inverse of the median of the relative error. The drawback of this estimator is that it can give too much weight to the numerous points where the fidelity is low just because there are lots of pixels without signal. We thus choose to compute four fidelity medians, taking into account only the pixels whose intensity in the initial model image is higher than 0.3, 1, 3.3 and 10% of the peak.

Fidelity range

The fidelity range has first been introduced by L. Kogan as:

$$\text{fidelity range} = \frac{\max(\text{abs}(\text{model}))}{\text{rms}(\text{difference})}$$

This estimator is close to the dynamic range when the model is mainly made of point sources. And it is close to the fidelity when the source is extended. Our experience is that the fidelity range follows the evolution of the fidelity medians, but with a less pronounced variation.

Fourier space estimators

An analysis in the *uv* plane is very convenient to straightforwardly identify which part of the Fourier space was measured or estimated by the observations. We thus computed the Fourier Transforms of the model and difference. We then define the *uv* fidelity as the ratio of those two images (note that the *uv* fidelity is not the Fourier Transform of the fidelity image). Since an interferometer is a spatial filter, we indicate in the figures presented below the limits of the area where visibilities can *directly* be measured by ALMA (the inner circle has a radius of 12 m and the outer circle has a radius of 150 m, the size of the ALMA configuration used in our simulations).

3 ALMA vs. ALMA+ACA

Figures 1 to 6 present the results of a set of simulations, performed with: *(i)* the ALMA array alone; *(ii)* the ALMA array complemented with single-dish observations providing the zero-spacing visibility; and *(iii)* the ALMA array complemented with the ACA array and single-dish observations providing the short spacings. The results are presented both in the image and *uv* planes. These simulations have the following properties:

- The input model image is an Hα map of M 51, which is well adapted to these simulation tests because it has structures at all spatial frequencies.
- A snapshot of a 7–fields mosaic (following an hexagonal pattern) at 230 GHz is simulated.

- ALMA is used in its compact configuration.
- ACA has 12 antennas of 7 m, with a north-south stretched random configuration. It observes four times longer than ALMA. It observes the same positions as ALMA, i.e. an oversampled mosaic.
- Four 12–m antennas are operated in single-dish mode to provide the short spacings. They observe the same time as ACA (i.e. 4 times longer than ALMA).
- These simulations are free of noise and pointing errors.

Note that a 7-fields mosaic is large enough to illustrate most of the effects occurring in wide-field imaging, as e.g. the lack of short spacing information, the influence of pointing errors, as well as the limitation of the mosaicing (reconstruction+deconvolution) methods.

Image quality improvement

The fidelities clearly follow the sequence: ALMA < ALMA + single-dish < ALMA + ACA + single-dish.

In theory, when observing a large mosaic with an interferometer, the visibilities at *all* spacings can be recovered (providing the *uv* coverage is dense enough): baselines down to the antenna diameter can be measured with the interferometer; in addition, it is a well-known result that mosaicing allows to recover visibilities down to the smallest baseline minus the antenna diameter. The simulations presented in this document do however show that such is not the case. This is especially well seen on the fidelity plots in the *uv* plane, which clearly show that ALMA alone cannot fill the central hole, even in mosaic mode. Adding the single-dish data allows to properly recover the information at the very center, but it is still surrounded by a ring-like gap. Only ACA provides the information required to properly estimate the visibilities at all scales. Several reasons can be invoked to explain why the homogeneous array concept does not seem to work efficiently: the reconstruction and deconvolution methods are limited; the recovered visibilities are attenuated by the antenna transfer function, which makes it difficult to recover the information at large *uv* distances; the mosaics need to be extremely large.

We therefore stress that, even for simulations of a "perfect" observation (no noise, no pointing errors), *adding the ACA observations definitely improves the image fidelity.*

Relative weighting

We performed a set of simulations with different weightings for the single-dish data, in order to assess the amount of time required by the single-dish as compared to the interferometric observations. The result actually slightly depends on the model image, which reflects the fact that the optimal combination depends on how the information is distributed over the *uv* plane. On average, the best results are obtained with:

ALMA	integration time $= t$
ACA	integration time $= 4t$
Single-dish	integration time $= 16t$

The integration time needed by the single-dish is simulated by 4 antennas observing $4t$ each, which seems a good compromize between the number of antennas and the required observing time.

4 Pointing errors

ACA and pointing errors

As described in the previous section, even in the lack of pointing errors, the inclusion of ACA data significantly improves the image fidelity. This effect is expected to be even more important when pointing errors are added.

An antenna in single-dish mode is sensitive to spatial frequencies u, v up to its diameter D, but the phase errors increase linearly with $\sqrt{u^2+v^2}$ and the pointing error. Similarly, an interferometer baseline u_0, v_0 is sensitive to the circle of diameter D centered on u_0, v_0, but the phase errors increase linearly with $\sqrt{(u-u_0)^2+(v-v_0)^2}$ and the pointing error; moreover, the sensitivity decreases quickly with increasing distance from u_0, v_0, and the noise is thus amplified. Finally, amplitude errors are important as well. All these effects are critical when trying to recover the u, v spacings between 0 and the shortest baseline (1.25×12 m) i.e. typically around 7 to 8 meters. Hence, adding the ACA data, which cover precisely this range in the uv plane is crucial for properly recovering all spatial frequencies.

Simulations

The simulations were done at a frequency of 230 GHz: in the absence of noise, the behaviour of the image quality at other frequencies can be derived by a simple scaling of our results.

We run a large number of simulations with various input parameters. Figure 7 compares the fidelity medians measured on the final images obtained with ALMA alone, ALMA + single-dish, and ALMA + ACA + single-dish. The fidelities measured with different intensity thresholds (0.3, 1, 3, and 10%) are presented as a function of pointing errors rms. Three different pointing error models were used: *(i)* only errors due to wind, with a correlation coefficient of 50% between antennas; (*ii*) only errors due to thermal deformation, including a drift with time, with a correlation coefficient of 70% between antennas; and (*iii*) both effects together. In the three cases, measurement errors were also present, and the total errors were normalized to get the same final rms (in practice: 0.6, 1.5, 3, and 6″ at 230 GHz). The pointing accuracy of 0.6″ is drawn as a vertical dash line in the upper right panel of Fig. 7, for an observing frequency of 230 and 690 GHz. The ACA antennas were assumed to have the same pointing error rms than the 12–m antennas, but with a different distribution: the measurement errors were assumed to be larger, while wind and thermal induced errors were smaller.

To compare the three images (ALMA, ALMA + single-dish , ALMA + ACA + single-dish), we were careful to use the *same* samples of pointing errors.

Results

Figure 7 clearly shows that adding the ACA observations does improve the median fidelities, by typically 50 to 100%. This effect is very pronounced when considering the brightest pixels. It is only marginal when using the pixels above 0.3% of the peak: this reflects that our simulation method is limited to maximum fidelities of ∼300 (see the simulation tool description).

Comparison with other works

In a recent memo, Morita found that ACA does not improve much the wide-field imaging capabilities of ALMA. He used MEM deconvolution techniques. To try to understand the disagreement between his results and ours, we also run a set of simulations on the image he used (M31), with the same ACA configuration (11×8 m). We also found that, on average, the improvement obtained by adding the ACA data is low. However, as can be seen on Fig. 8, the improvement increases when the median fidelity is computed on the pixels with the highest intensities. So our first guess it that the intensity threshold used by Morita to compute fidelities is too low.

Another point to consider is that the ACA configuration that was used (a regular ring) might be too regular to allow a good improvement in the deconvolution process. We thus tried to use our ACA configuration (north-south stretched random configuration of 12×7–m antennas). Fig. 9 shows that the improvement due to ACA systematically increases with this random configuration as compared to the regular ring configuration. We don't know yet whether this is an effect of the antenna diameter or of the configuration.

Finally, we note that the Fourier Transform of the M31 image has smoother properties between 0 and 12 meters than the M51 image. Hence, with only ALMA and the single-dish information, it is easier for the deconvolution algorithm to interpolate the 6 m information in the M31 case than in the M51 one. Adding the ACA information is thus less crucial in this particular case.

5 Other considerations

ACA calibration

Calibration may become a limiting factor when the ACA is operated, as its sensitivity is much lower than that of ALMA. The observations of point-like sources (quasars) are required to calibrate the pointing, focus, bandpass, as well as the time evolution of the amplitude and phase. The calibration sensitivity goes as $\sqrt{n}D^2$. Hence, if a good calibration is achieved with ALMA (60 antennas of 12 meters) on a 0.1 Jy source, then ACA (e.g. 12 antennas of 7 meters) require a 0.7 Jy calibration source. This discrepancy will obviously have serious consequences on the calibration accuracy achieved with ACA. A very efficient way to reduce this limitation is to add a few 12–m antennas to ACA for the calibration. Adding 4 12–meters antennas to ACA for the calibration, push down the limit to 0.45 Jy.

A possible operation scheme

The number of single-dish antennas needed to complement the ALMA or ALMA + ACA data as well as the ACA calibration problem strongly suggest that four 12–m antennas should be permanently dedicated to the short spacings measurements and to the ACA calibration. Since both ACA and the single-dish measurements require an integration time four times longer than ALMA, the following operation scheme can be proposed:

- During 25% of the time, ALMA observe sources requiring short spacing information.
- During 100% of its time, ACA and the single-dish antennas measure the short spacings required to complement these ALMA observations. Hence, a ratio 1:4 between the ALMA and the ACA/single-dish integration time is obtained.
- The ACA and single-dish observations are synchronized, such that the 12–m antennas can be used with ACA when a calibration observation has to be performed.
- During the remaining 75% of its time, ALMA observes the projects that do not require the inclusion of short spacings, i.e. small-field high-angular resolution studies (e.g. protostellar disks, high-z source surveys).

The consequences of such an operation mode are the following:

- Only four 12–m antennas have to be equipped with wobblers.
- ALMA is a 60 antennas array. The configuration have to be optimized for 60 antennas.
- Two correlators are needed: one for ALMA (60 antennas), and one for ACA (12 antennas in the example studied here, plus four 12–m antennas).

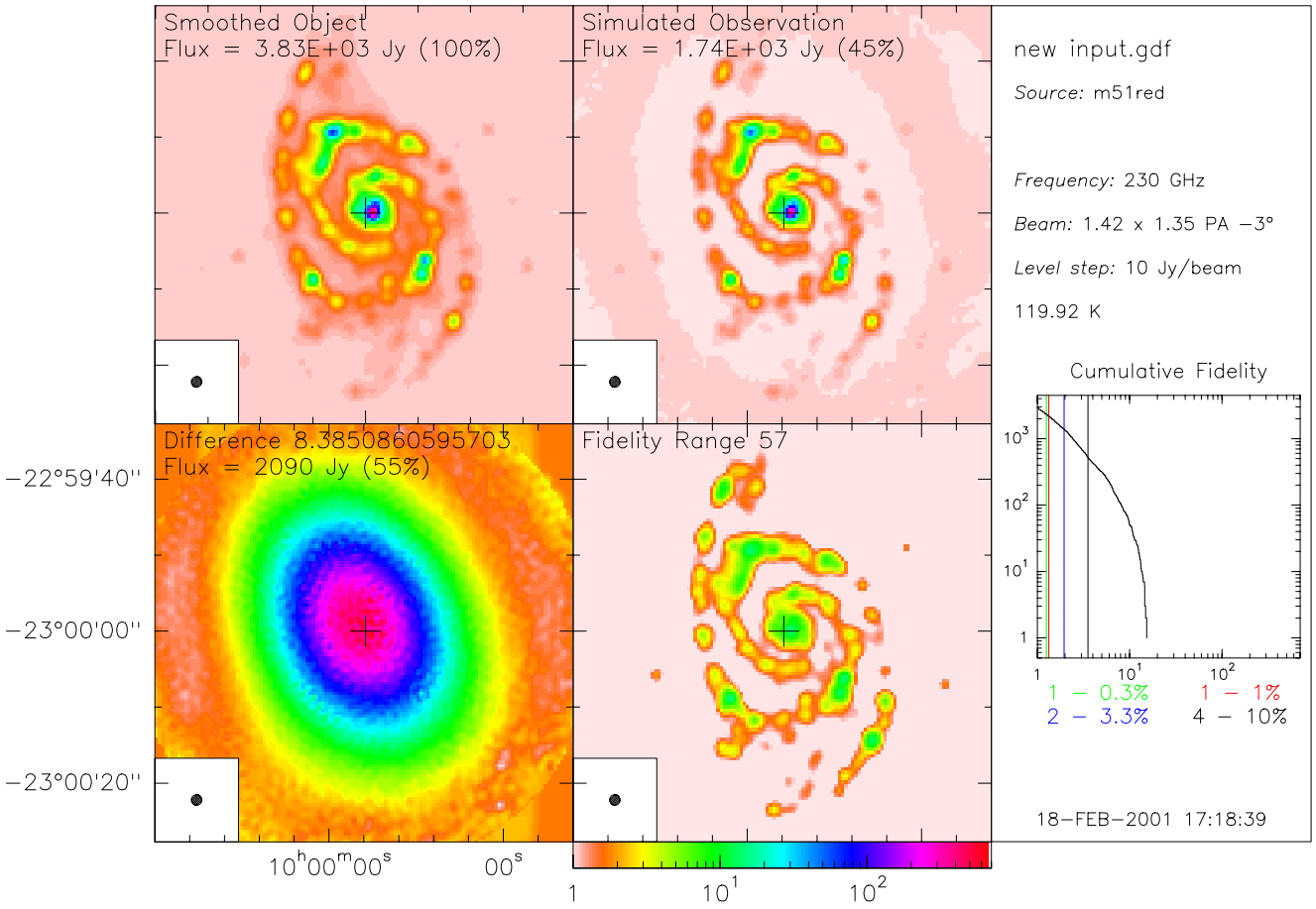

Figure 1: Simulation of observations made with the ALMA array alone. The simulated observation is a snapshot (0.3 hour) of a 7–fields mosaic following an hexagonal pattern. The 2 top images show the model (right) and the simulated observation (left), both smoothed at the same resolution. The 2 bottom images show complementary information: the difference (model−simulation, at left) and the fidelity (model/(model−simulation), at right). To quantify the visual impression, several numbers are provided: integrated fluxes (and their percentage as compared to the model); rms of the difference image; fidelity range. Finally the histogram of cumulative fidelity is shown with median fidelities computed for the image pixels whose intensity is at least 0.3/1/3.3/10% of the maximum value.

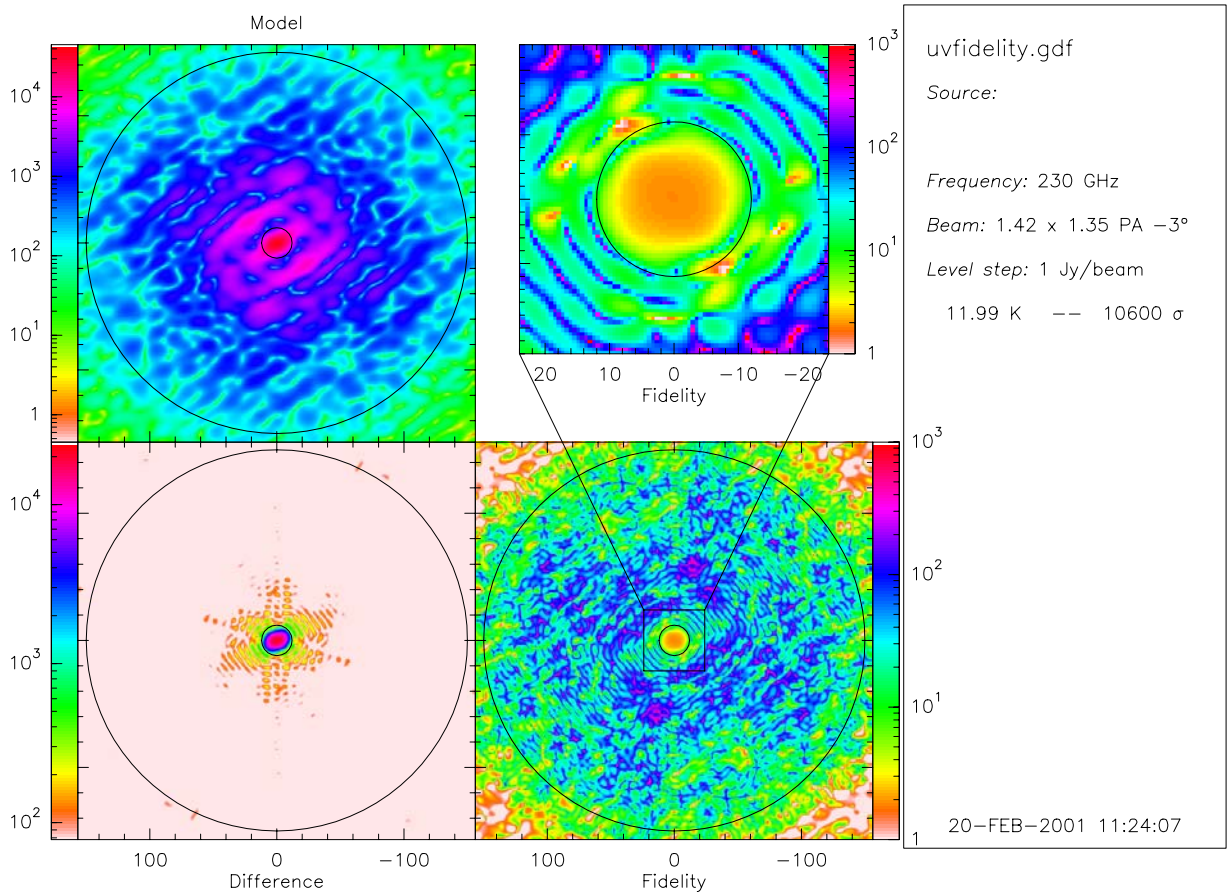

Figure 2: Idem than Fig. 1 but the results are shown in the Fourier plane. The top left corner show the FFT of the model. The bottom left corner the FFT of the difference (model−simulation). The bottom right corner is the ratio of the 2 previous FFTs: this is an image of the fidelity of the observation in the *uv* plane. Finally, the top right panel is a zoom of the *uv* fidelity. The large circle enclose the region where visibilities where measured (its radius is the size of the ALMA configuration, 150 m). The small 12 m circle enclose the area where ALMA can a priori make only indirect visibility measurement (via mosaicing). Note that in this circle the *uv* fidelity is very low.

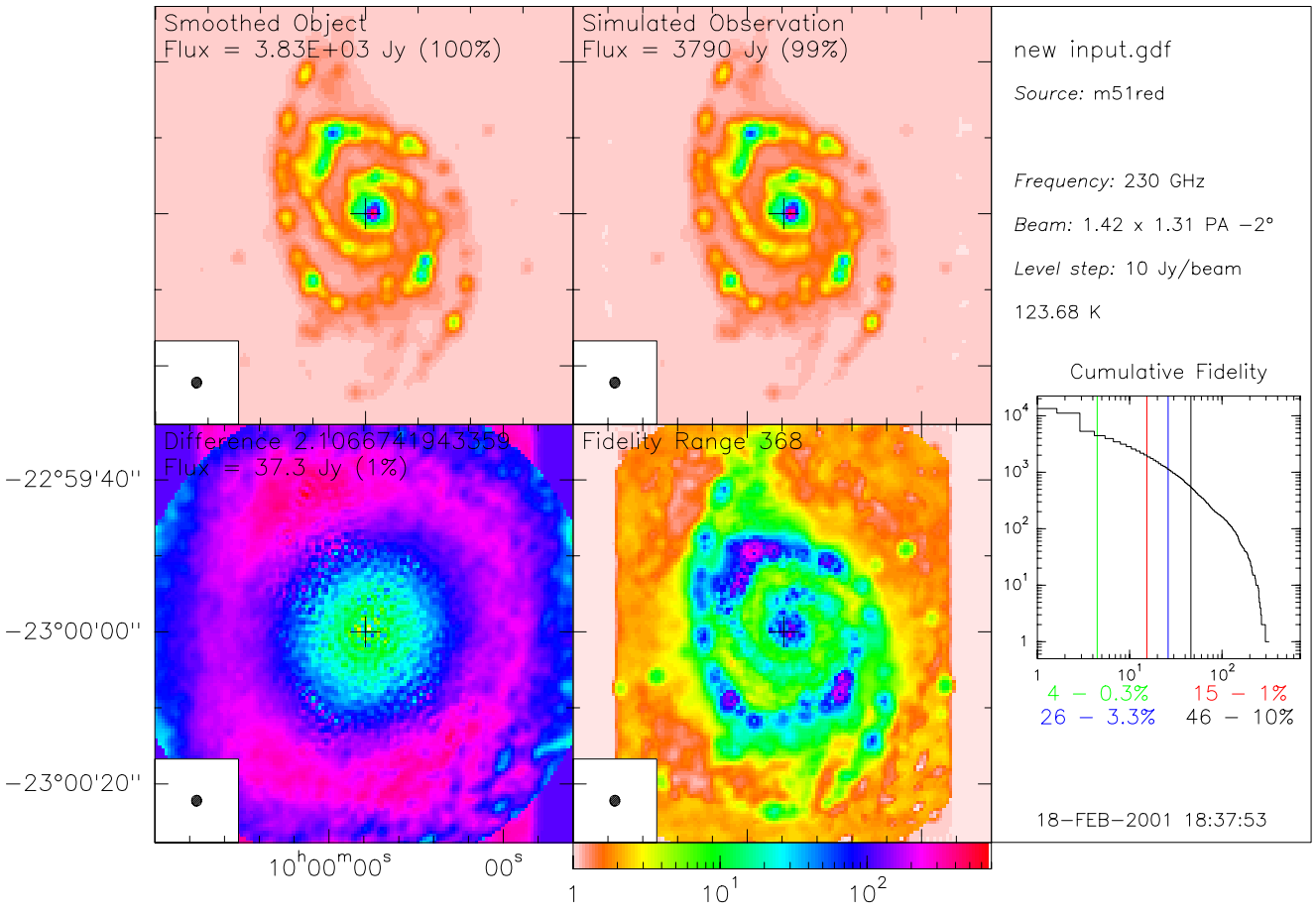

Figure 3: Idem than Fig. 1, for a simulation with the ALMA array and single-dish (4 antennas observing 4 times longer than ALMA) providing the zero spacing. The flux is properly recovered and the fidelity has considerably increased.

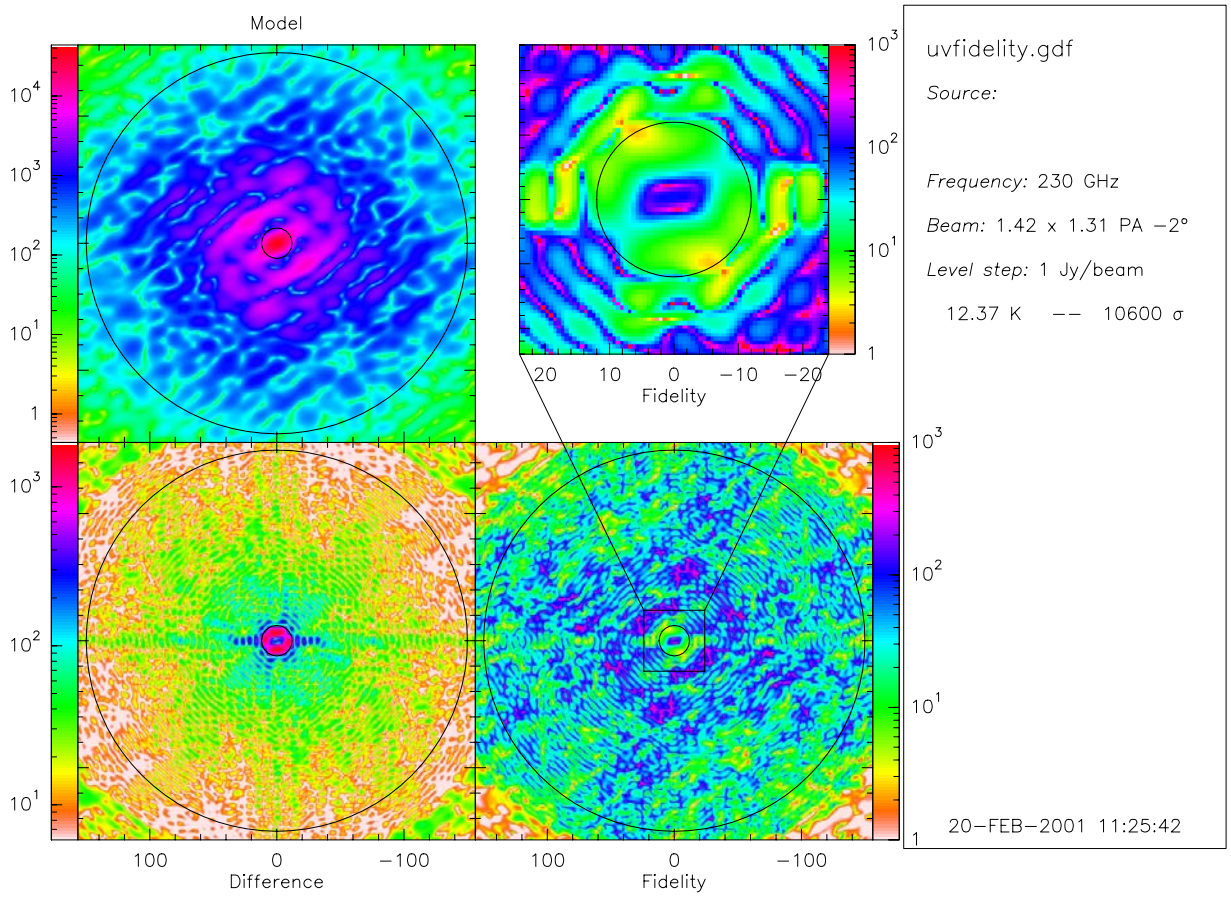

Figure 4: Idem than Fig. 2, for a simulation with the ALMA array and single-dish (4 antennas observing 4 times longer than ALMA) providing the zero spacing. Note that the *uv* fidelity around zero is now very high but the fidelities around 6 m are still very low, indicating that those visibilities were not properly recovered.

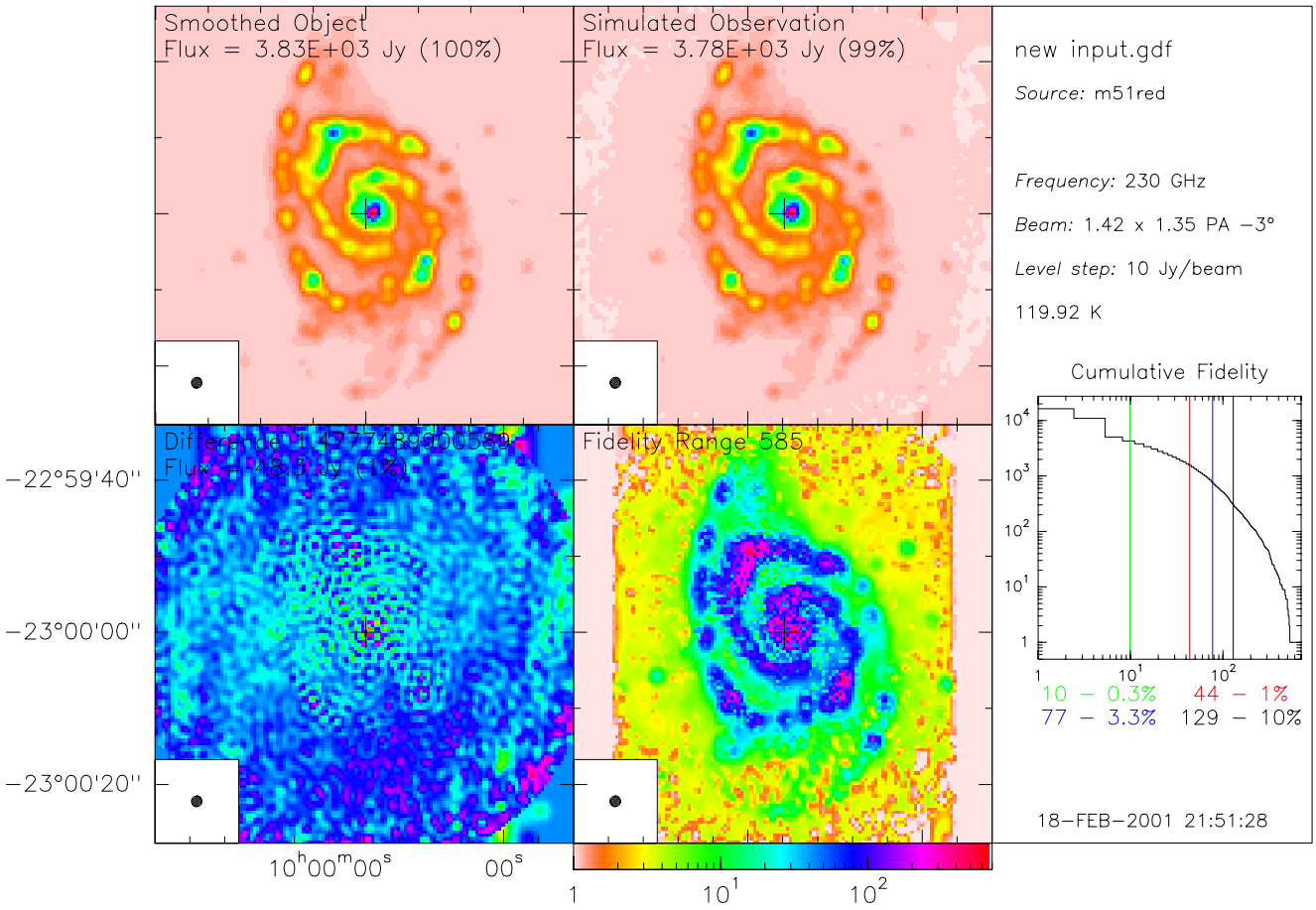

Figure 5: Idem than Fig. 1, for a simulation with the ALMA array, the ACA array (12 7–m antennas observing 4 times longer than ALMA), and single-dish providing the short spacings. Large scale structures disappear on the difference image and the median fidelities are increased by at least a factor 2.

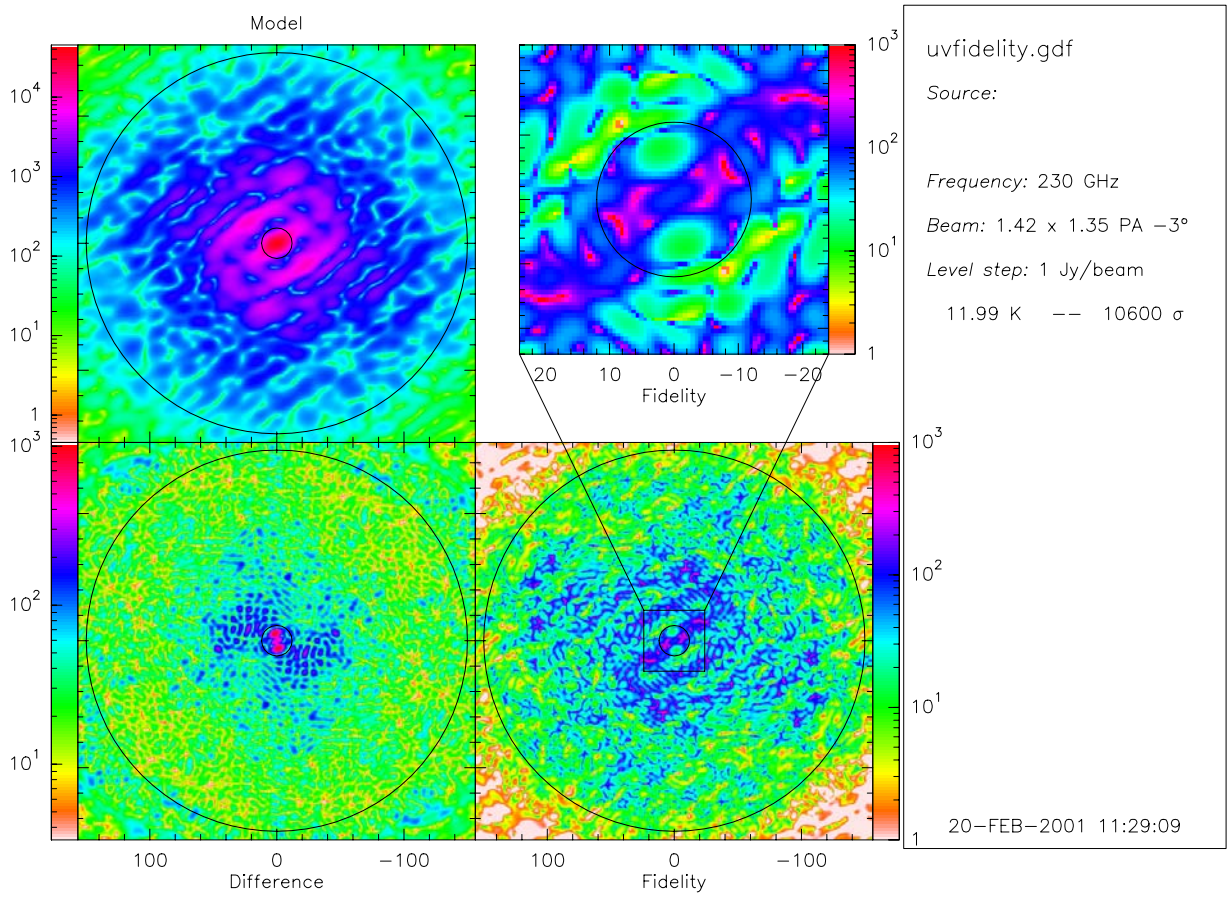

Figure 6: Idem than Fig. 2, for a simulation with the ALMA array, the ACA array (12 7–m antennas observing 4 times longer than ALMA), and single-dish providing the short spacings. The *uv* fidelity is now continuously high at all the low spatial frequencies.

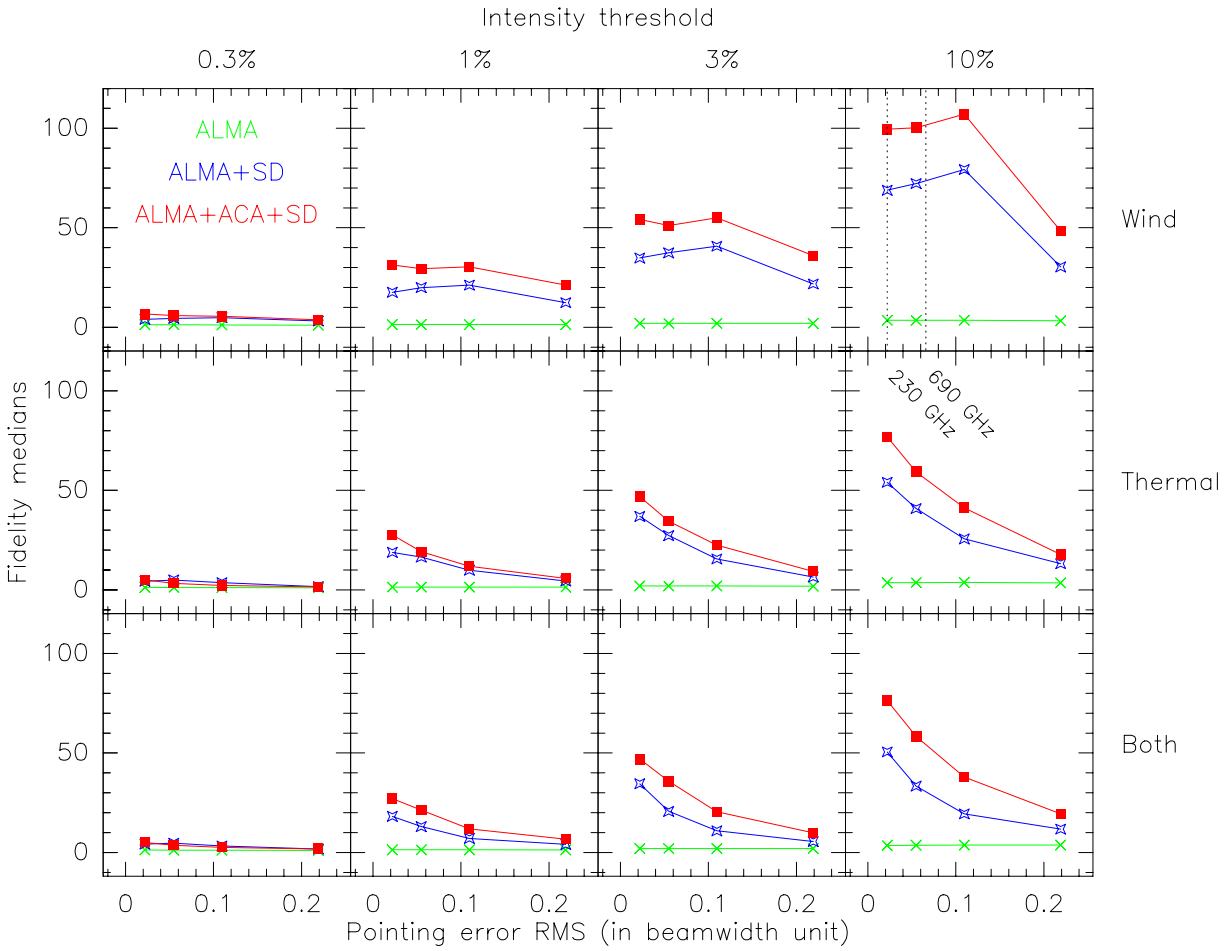

Figure 7: Fidelity medians estimated above 0.3, 1, 3 and 10% of the model intensity peak, as a function of the pointing error rms. The input image is the M51 map. Three models of pointing errors are compared (see text). The 0.6" pointing error specification of the ALMA antennas is drawn as dash vertical lines in the upper right panel, for observing frequencies of 230 and 690 GHz.

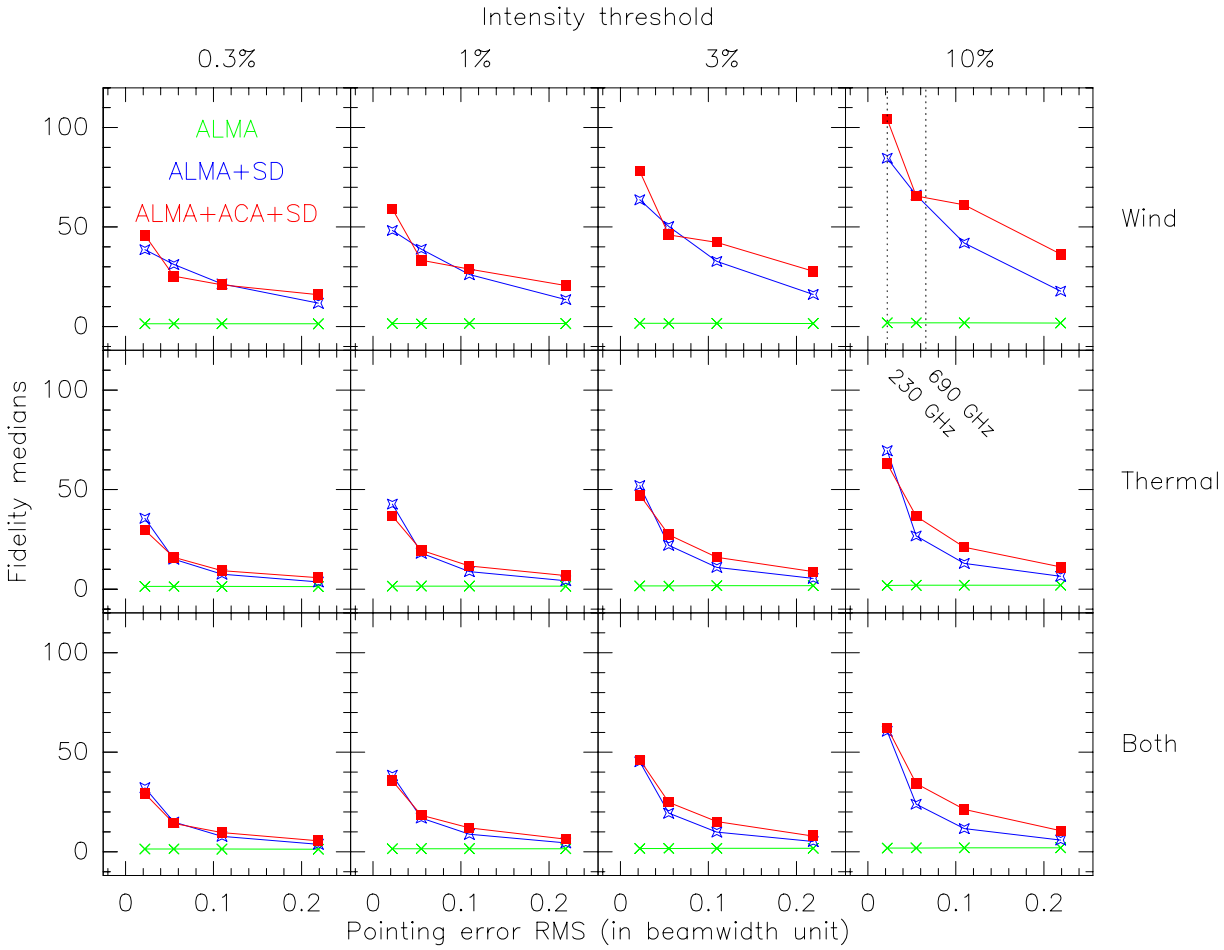

Figure 8: Fidelity medians as a function of the pointing error rms (see Fig. 7), computed on simulations of the M 31 model image. The ACA is here an 11×8 m array (regular ring configuration used by Morita). Adding the ACA data improves the image fidelity only when the median is computed on the brightest pixels.

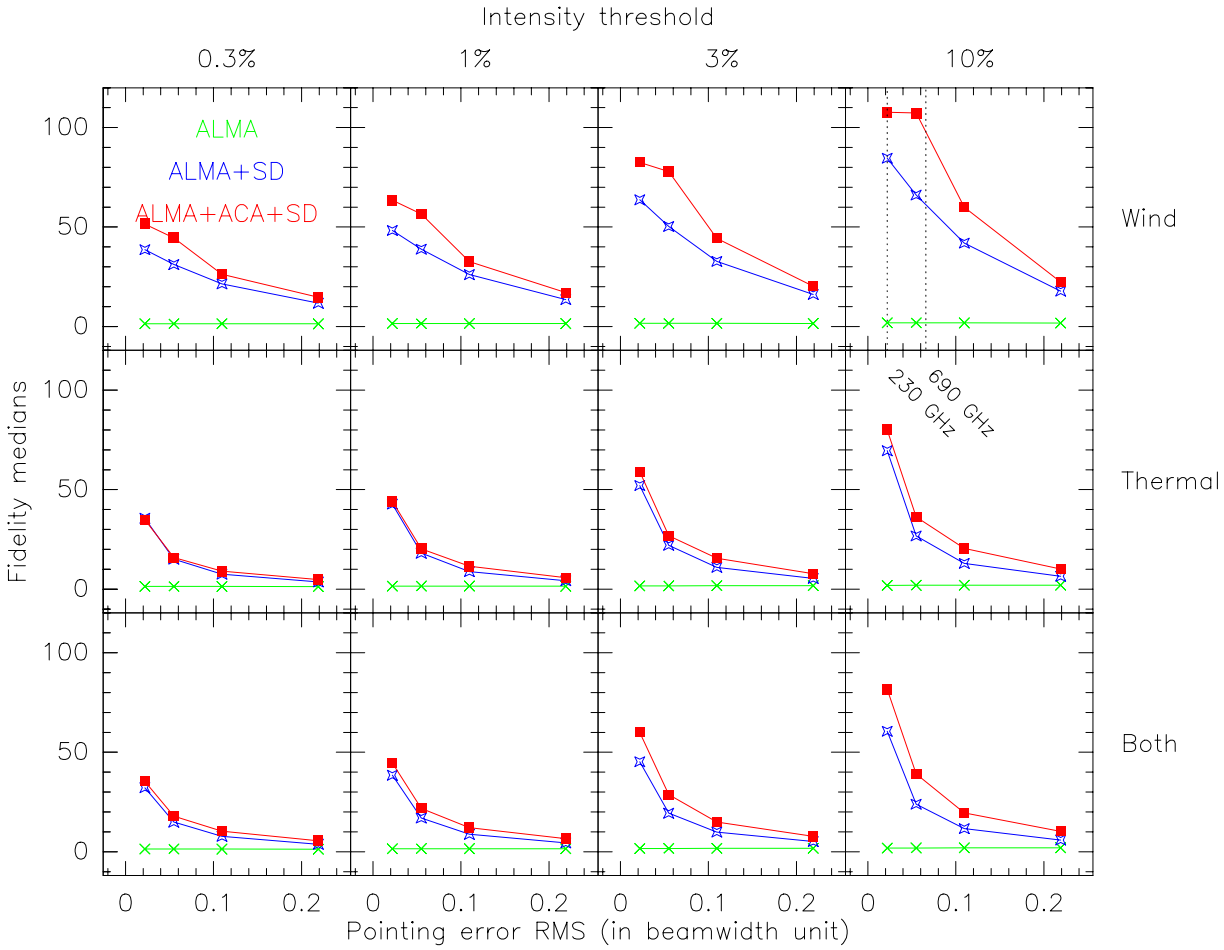

Figure 9: Fidelity medians as a function of the pointing error rms (see Fig. 7), computed on simulations of the M 31 model image. The ACA is here an 12×7 m array (random configuration used in this memo). In this case, ACA systematically improves the image fidelity.